[Journal of Geophysical Research, Solid Earth]

Supporting Information for

[Spatial changes in gas transport and sediment stiffness influenced by regional stress: observations from piezometer data along Vestnesa Ridge, eastern Fram Strait]

[Andreia Plaza-Faverola[1]; Nabil Sultan[2]; Renata G. Lucchi[3]; Naima El bani Altuna[1]; Hariharan Ramachandran[1]; Sunny Singhroha[1]; Frances Cooke[1]; Sunil Vadakkepuliyambatta[4]; Mohamed M. Ezat[1]; Tine L. Rasmussen[1]]

[1-CAGE-Centre for Arctic Gas Hydrate, Environment, and Climate, Department of Geosciences, UiT-the Arctic University of Norway, Tromsø, Norway
2-Geo-Ocean, UMR6538, Ifremer, CNRS, UBO, UBS, 29280 Plouzané, France
3- National Institute of Oceanography and Applied Geophysics – OGS, Trieste, Italy
4- National Centre for Polar and Ocean Research, Ministry of Earth Sciences, Vasco-da-Gama, Goa, India]

Contents of this file

Text S1 – oedometer tests

Oedometer tests were conducted at wholearound sub-samples from 2 depth intervals along each core using a constant rate of strain (CRS) [*ASTM International*, 2006] at the labs by the Norwegian Geotechnical Institute (NGI). In addition, oedometer tests with incremental loading were performed on ten samples (Table S 1) using incremental loading according to the ASTM D-2435 method [*Astm*, 2004]. The aim is to characterize both the consolidation/compressibility characteristics and permeability. During incremental consolidation tests, the falling-head method is used to determine the permeability (or hydraulic conductivity) of the sediment samples. Sediment samples were selected from two different sites (C-05 and C-12 – Figure 1 main text) investigated during the CAGE 19-3 cruise of RV "Kronprins Haakon" [*Knies and Vadakkepuliyambatta*, 2019]. The two sites were chosen near the piezometers Pzm05 and Pzm12W deployed to characterize the in-situ thermal and hydraulic regimes.

Table S1 indicates the characteristics of the ten tests carried out on two sediment Calypso cores (C-05 and C-12). Column four in Table S1 specifies the quality of the tested samples based on the criteria in [*Lunne and Long*, 2006]. Based on MSCL P-wave and ρ-density log data, six samples were selected from site 5 (black horizontal triangles in Figure S1) and four samples from site 12 (black horizontal triangles in Figure S2). Depths at which the samples were selected correspond to the position of six sensors of the piezometer Pzm5 and four sensors of the Pzm12W (red dash lines in Figure S1 and Figure S2).

Figure S3 summarizes the experimental results of the CRS oedometer test showing the change of the void ratio as a function of the axial effective stress.

Figures S4 and S5 summarizes the experimental results of the oedometer tests (incremental loading) with the void ratio, permeability and coefficient of consolidation versus effective axial stress.

Figures S3 to S5 show the data used to determine the compressibility indexes (*Cc)*.

Text S2 – sedimentological data

Sedimentological data from calypso cores C-4, C-12 and C-5 are shown in Figures S6 to S8. Bulk density, P-Wave velocity, XRF mineral ratio logs, water content, and the visual core description, are included in addition to grain size and magnetic susceptibility presented in figure 2 in the main text.

Text S3 – piezometer data

As shown in Figure 3, most of the pore-pressure dissipation curves did not reach the equilibrium pressure (Δu_{eq}). The modified cavity expansion approach proposed by [*Sultan and Lafuerza*, 2013] aims to simulate this pore water dissipation process from partial measurements of the in-situ pore water pressure. The details on the method are described in Sultan and Lafuerza [2013] for the cylindrical and spherical cases. Hereby we include the main equations and the numerical approach used for the cylindrical expansion case where the dissipation of Δu(r,t) with time is calculated using the following consolidation equation [*Burns and Mayne*, 1998]:

$$\frac{\partial(\Delta u)}{\partial t} = \frac{C_h}{r}\frac{\partial(\Delta u)}{\partial r} + C_h\frac{\partial^2(\Delta u)}{\partial r^2} \qquad \text{(eq S1)}$$

Where r varies between r_0 the radius of the piezometer rod and r_p the radius of the sheared and plasticized zones determined using the cavity expansion theory [*Burns and Mayne*, 1998]:

$$r_p = r_0\sqrt{I_r} = r_0\sqrt{\frac{G}{Su}} \qquad \text{(eq S2)}$$

Where S_u is the undrained shear strength and G is the shear modulus.

In the approach by Sultan and Lafuerza [2013], the coefficient of consolidation C_h is considered to change linearly during the dissipation process (from C_{hi} to $(1-\beta)\,C_{hi}$) and it decreases with time according to the following equation [*Abuel-Naga and Pender*, 2012]:

$$C_h = C_{hi}\left[1 - \beta\frac{\Delta u_i - \Delta u}{\Delta u_i - \Delta u_{eq}}\right] \qquad \text{(eq S3)}$$

Where Δu is excess pore pressure and β corresponds to the Abuel-Naga and Pender [2012] "icv" dimensionless parameter. β(=icv) describes the change of the coefficient of consolidation with the consolidation stress increment. The aim of this method is to predict accurately the Δu_{eq} integrating partial dissipation tests. In order to fulfil this main goal, equations S1 to S3 were numerically solved by approximating all the derivatives by finite differences and by using an explicit numerical method. A numerical scheme similar to the one proposed by [*Kim and Lee*, 2000] was implemented (Figure 3) and solved using the fortran programming language. The calculation of the excess pore pressure evolution with time at a given sensor leads to consider numerically the change in Δu in space r (with $r_0 \le r \le r_p$) and time t (with $t \ge 0$). In addition, the numerical calculation requires the specification of boundary conditions at $r = r_0$ and $r = r_p$, and initial conditions at time t = 0. The limit conditions are as follow: impermeable wall at $r=r_0$ and $\Delta u=\Delta u_{eq}$ at $r=r_p$. At t=0, the pore pressure Δu_i at $r=r_0$ is measured by the piezometer and considered as an input in the calculation.

An iterative procedure is necessary to determine the more appropriate values for the unknowns of the problem (C_h, β, Ir and Δu_{eq}) by means of an optimization algorithm. This becomes a numerical problem that consists in finding a set of variables that gives the minimum error between measured and predicted pore pressure at a given sensor. The uniqueness of the solution and therefore the correctness of the prediction of the unknowns depend on the time length of the dissipation test. Sultan and Lafuerza [2013] defined the following criterion to accurately calculate the in-situ equilibrium excess pore pressures (Δu_{eq}): the second derivative of pore pressure, Δu, versus the logarithmic of time, t, must be positive $\left(\frac{\partial^2\Delta u}{\partial ln(t)^2} > 0\right)$. They also showed that a dissipation pore-water pressure curve matches with a unique value of $\frac{C_h}{\sqrt{I_r}}$ that may correspond to infinite couples of "rigidity index - I_r" and "hydraulic diffusivity - C_h". It becomes therefore impossible to derive I_r and C_h for unknown sediments from a dissipation pore-water pressure curve alone [*Sultan and Lafuerza*, 2013].

In this study, the cavity expansion method developed by Sultan and Lafuerza [2013] was applied for 35 dissipation curves where the $\frac{\partial^2 \Delta u}{\partial ln(t)^2}$ criteria was fulfilled (Figures S5 to S9). For 3 dissipation curves, the recording time was not long enough to perform the calculation (Figures S8 and S9). For Pzm5 (Figure S5), the upper pore pressure curves were very noisy (i.e., strong pressure fluctuations) to be analyzed. The calculation results in Figures S5 to S9 show that for an average of three calculation runs per sensor (red, blue and green curves), the dissipation solution was almost unique with very low variability in Δu_{eq} and $\frac{C_h}{\sqrt{I_r}}$ (Figure 4).

Text S4 – Methane solubility

The methane solubility at the bottom simulating reflection (BSR) depth at both sites Pzm5 and Pzm4W was calculated using the method of [*Spivey et al.*, 2004] by considering the salinity, temperature and pressure conditions at the base of the BSR. The temperature was calculated by considering a permanent thermal regime (constant thermal gradient) and the seabed temperature (Figure S14). The pressure was calculated by assuming hydrostatic conditions. For Pzm5 (depth=170 mbsf; T= -1.05°C; salinity= 34.5 g/L), the methane solubility χ is found to be equal to 123 mM while for the Pzm4W conditions (depth=200 mbsf; T= -0.95°C; salinity= 34.5 g/L) χ is equal to 126 mM (Figure S14).

Text S5 – Δu versus tide cycles

The data collected from Pzm5 provide insights into the variation of the Δu values with tide cycles. Although one would expect that the use of differential pressure sensors will eliminate the effects of tide cycles on the measured Δu, observed perturbations occurring during the low and ascendant tide cycle phases suggest that the dynamics of free gas, which increases the compressibility of the pore fluid, is affecting the pore pressure measurements (Figure S15). Red periods in Figure S15-a correspond to gas exsolution and expansion while black periods indicate gas dissolution and compression. The perturbation of Δu is expected to be proportional to the gas content [*Garziglia et al.*, 2021].

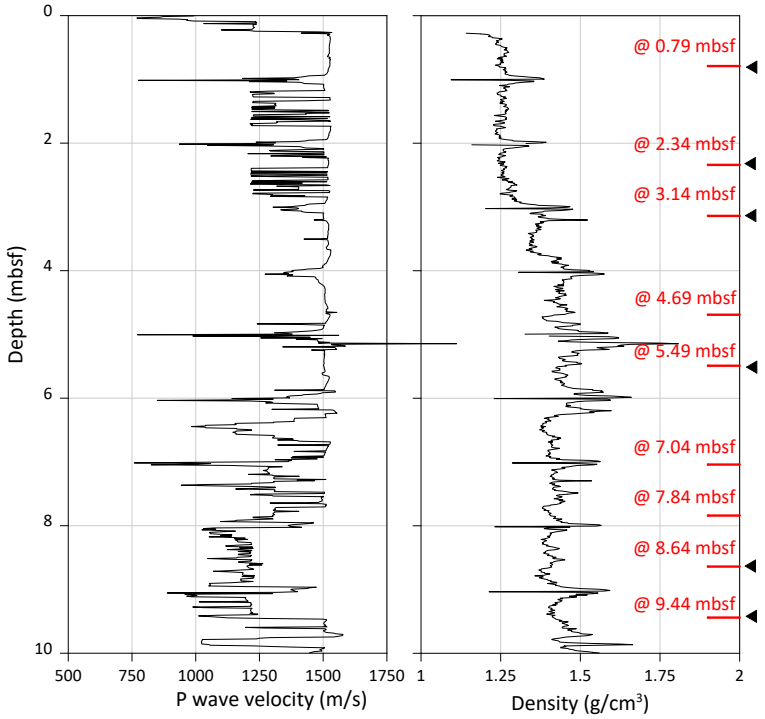

Figure S1. Core C-05. Six samples selected to carry out oedometer tests based on core P wave and ρ-density log data.

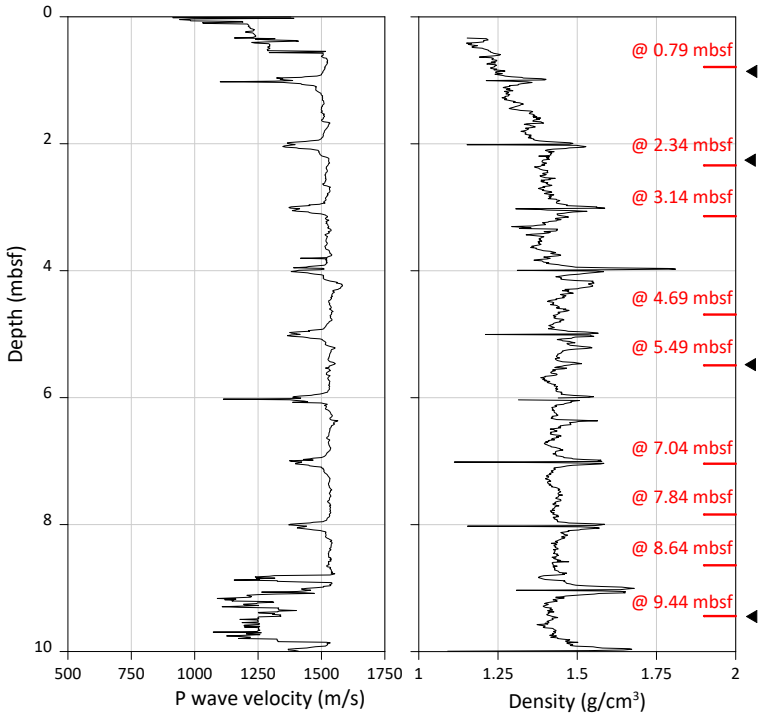

Figure S2. Core C-12. Six samples selected to carry out oedometer tests based on core P wave and ρ-density log data.

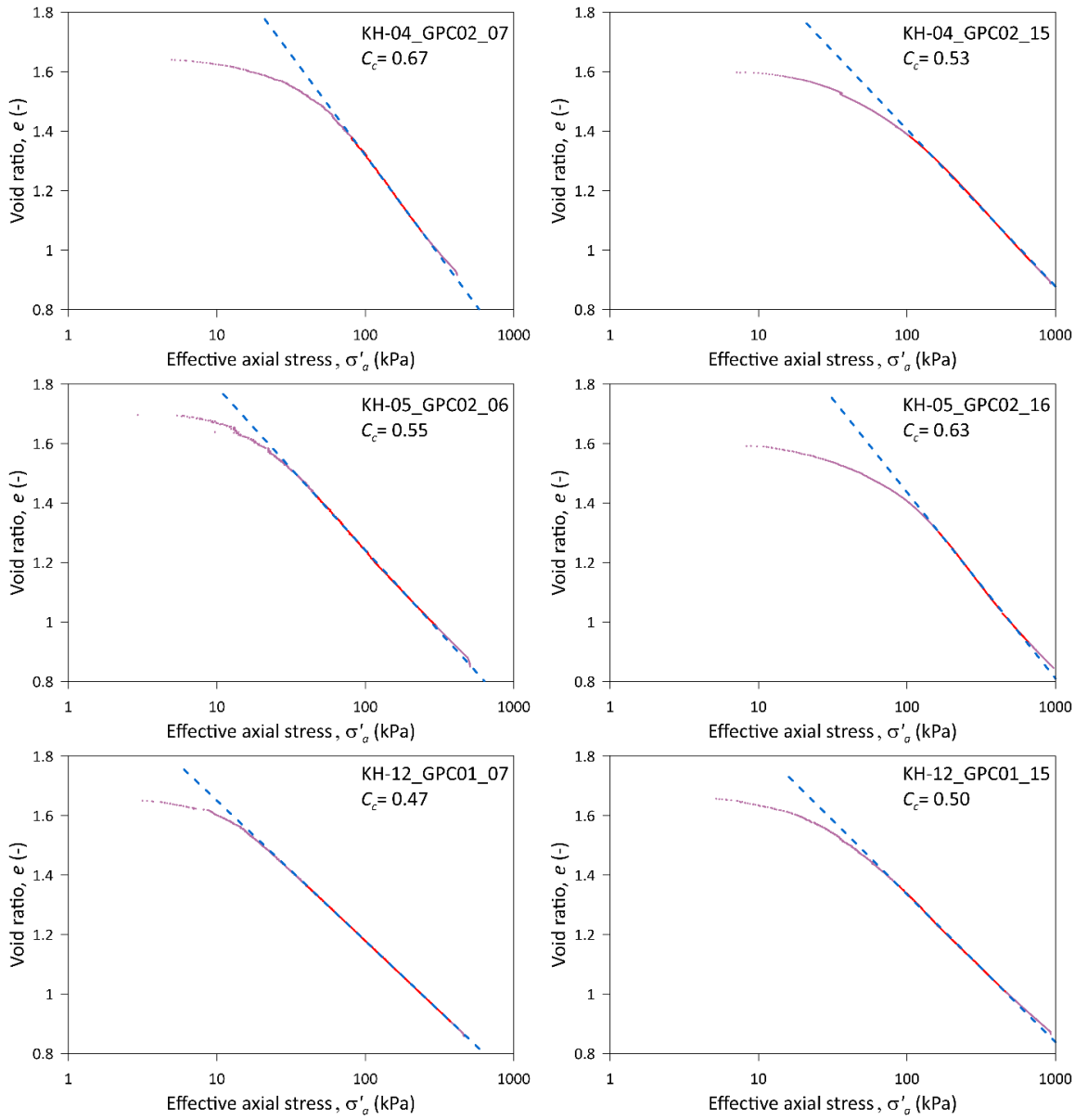

Figure S3. Summary of one dimensional oedometer tests (CRS).

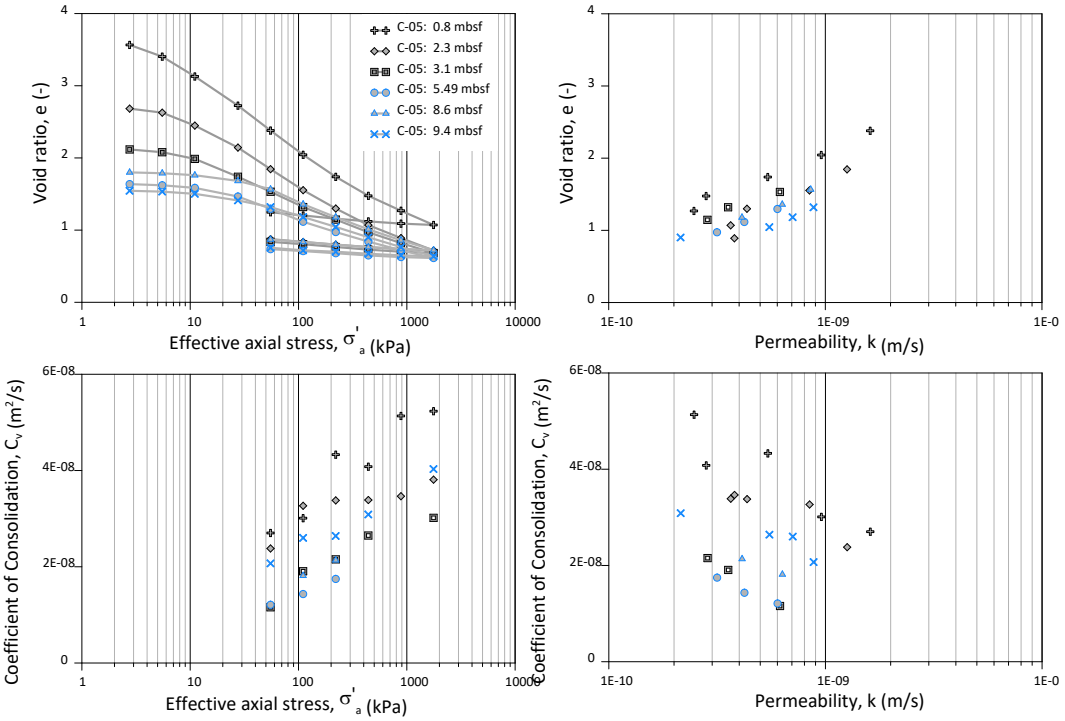

Figure S4. Core C-05. Summary of one dimensional oedometer tests (incremental loading).

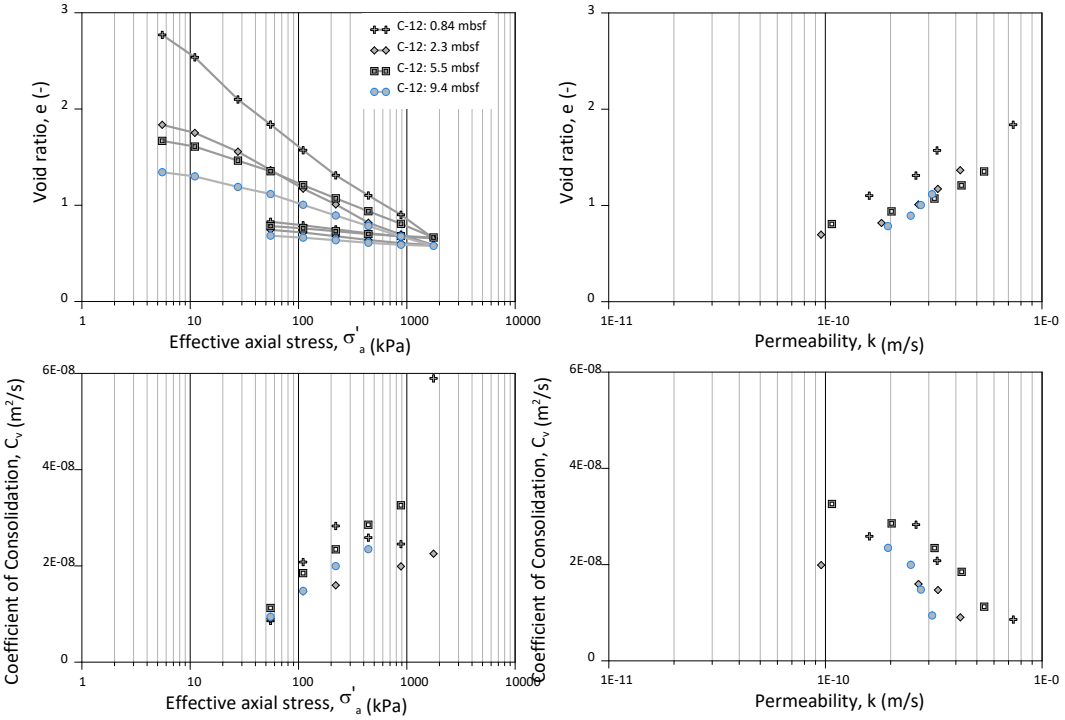

Figure S5. Core C-12. Summary of one dimensional oedometer tests (incremental loading).

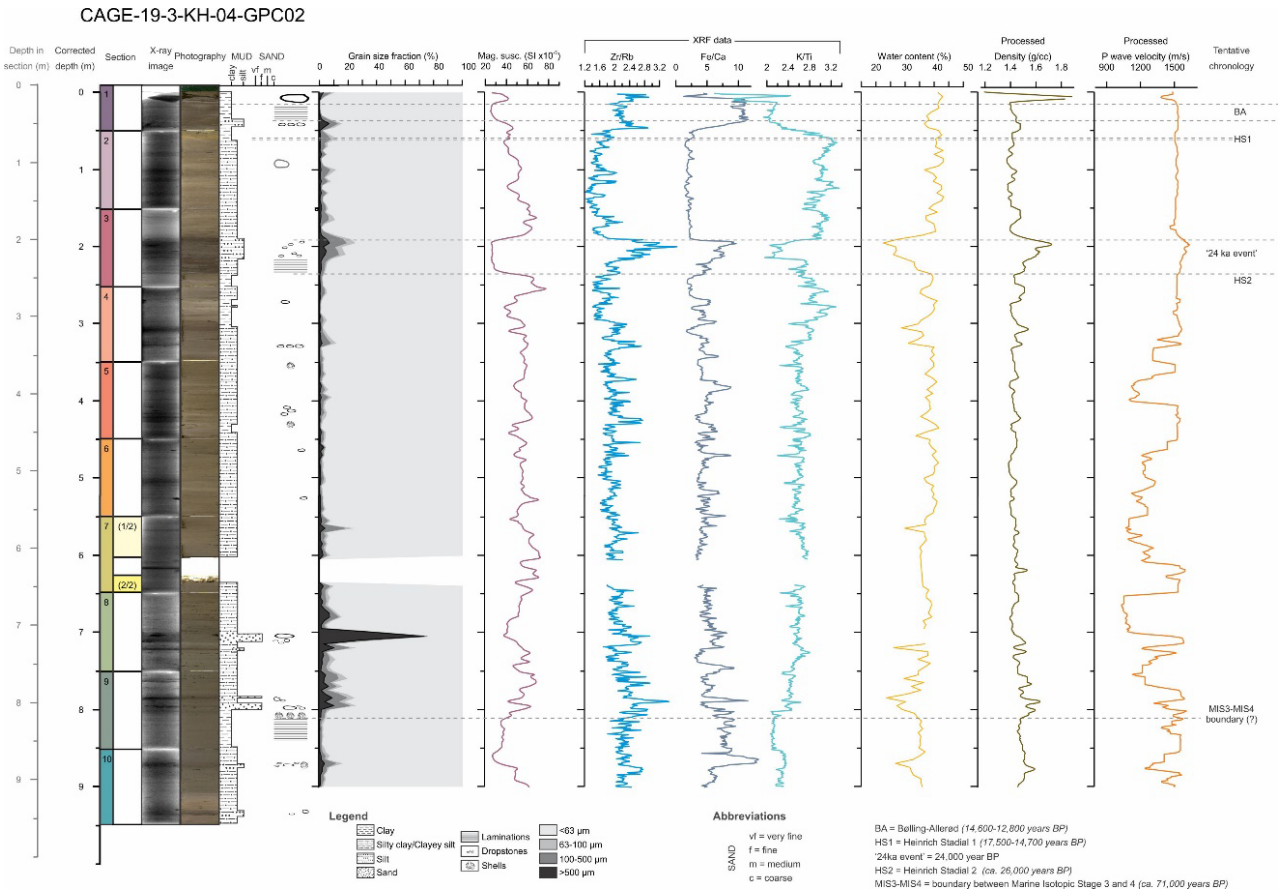

Figure S6. Additional sedimentological data from calypso core C-4. Bulk density, P-Wave velocity, XRF mineral ratio logs, water content, and the visual core description, are included in addition to grain size and magnetic susceptibility presented in figure 2 in the main text.

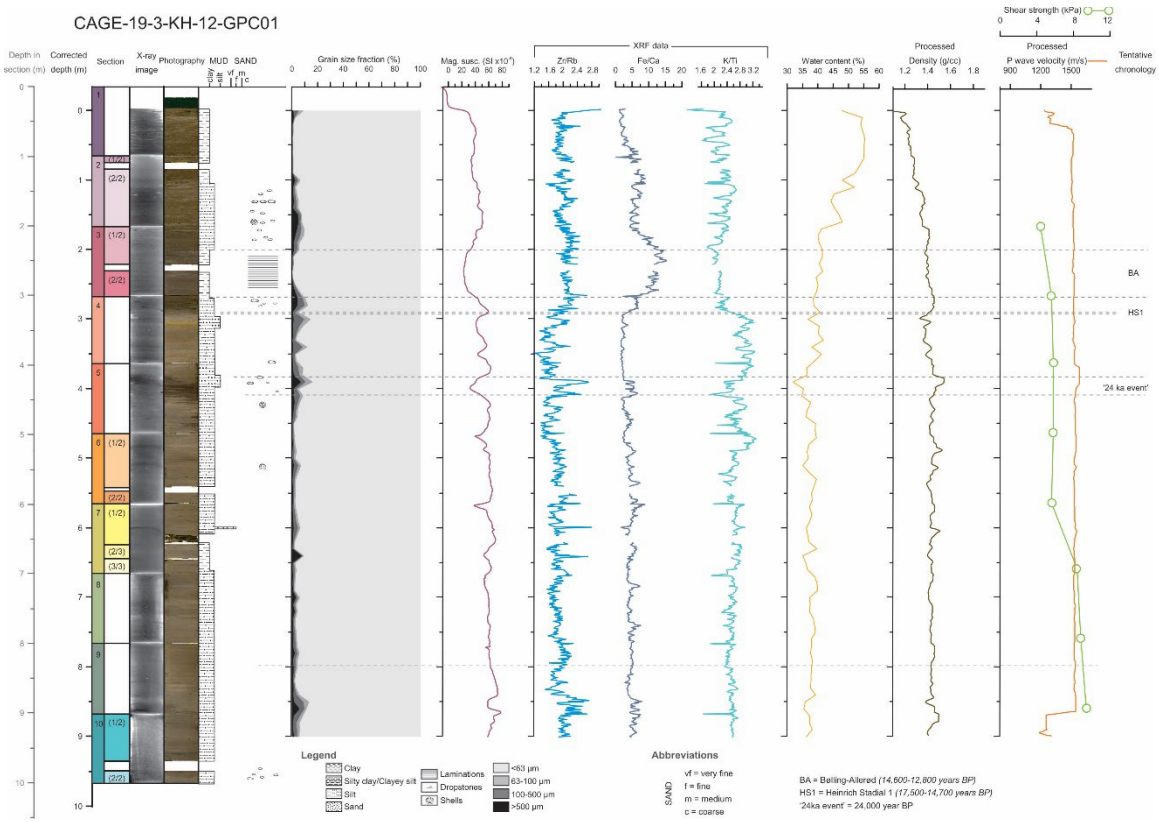

Figure S7. Additional sedimentological data from calypso core C-12. Bulk density, P-Wave velocity, XRF mineral ratio logs, water content, and the visual core description, are included in addition to grain size and magnetic susceptibility presented in figure 2 in the main text.

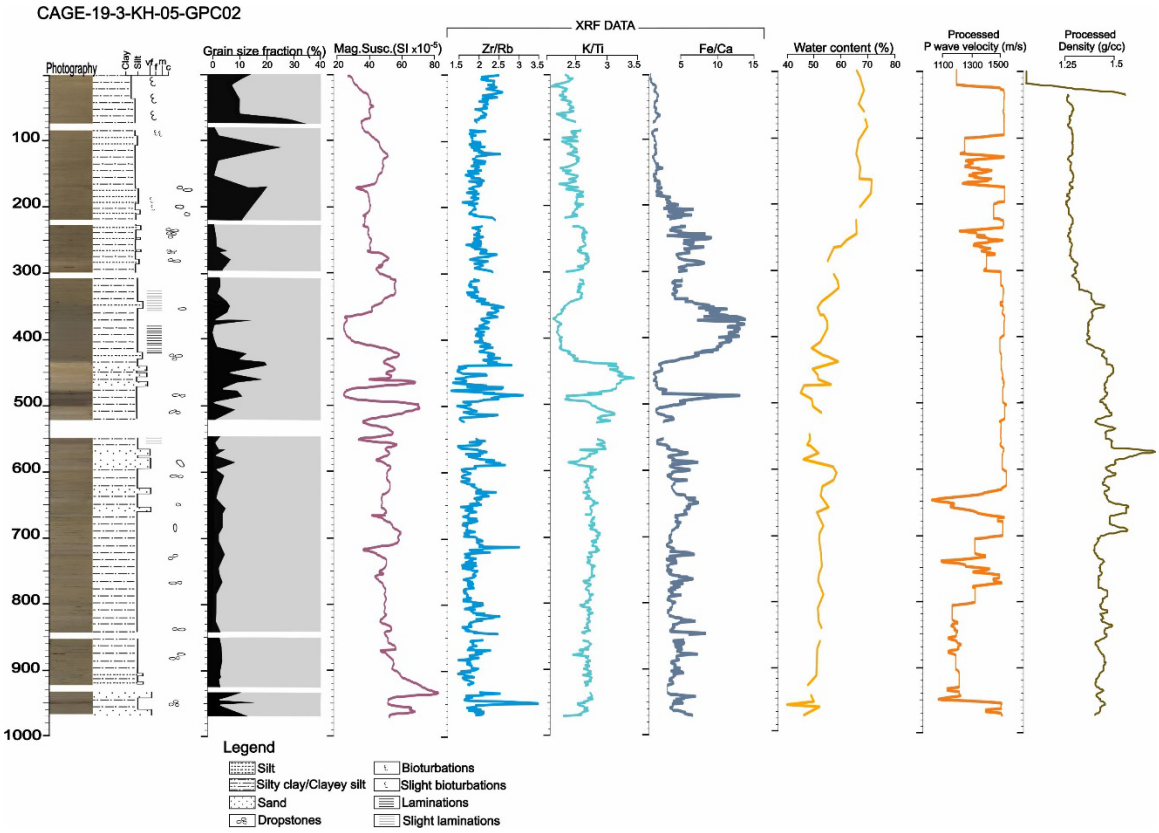

Figure S8. Additional sedimentological data from calypso core C-5. Bulk density, P-Wave velocity, XRF mineral ratio logs, water content, and the visual core description, are included in addition to grain size and magnetic susceptibility presented in figure 2 in the main text. The grain size analyses for the upper 2 m has a poor sampling rate of 20 cm and has a large uncertainty associated. The apparent increase in the percentage of sediment > 63 µm is not necessarily representative of the sediment distribution of the sequence Holocene period along this core.

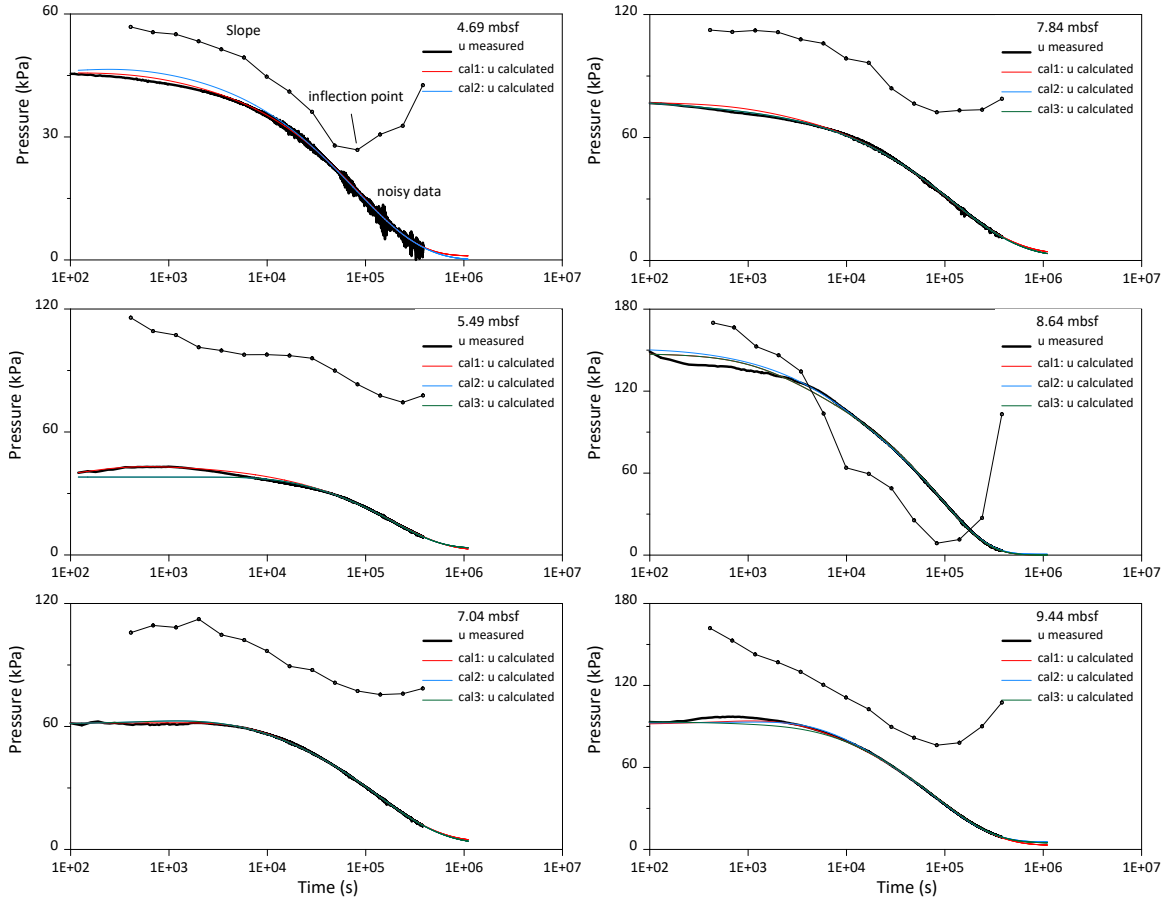

Figure S9. Pzm5. Three runs for the six deepest sensors with three different set of parameters giving similar pore-water dissipation curves. The full range of pore-water pressure dissipation data are also plotted (black line). $\frac{\partial \Delta u}{\partial(\ln(t))}$ values are added to the diagram showing for some sensors the inflection point which corresponds to the $\left(\frac{\partial^2 \Delta u}{\partial ln(t)^2} > 0\right)$ criteria.

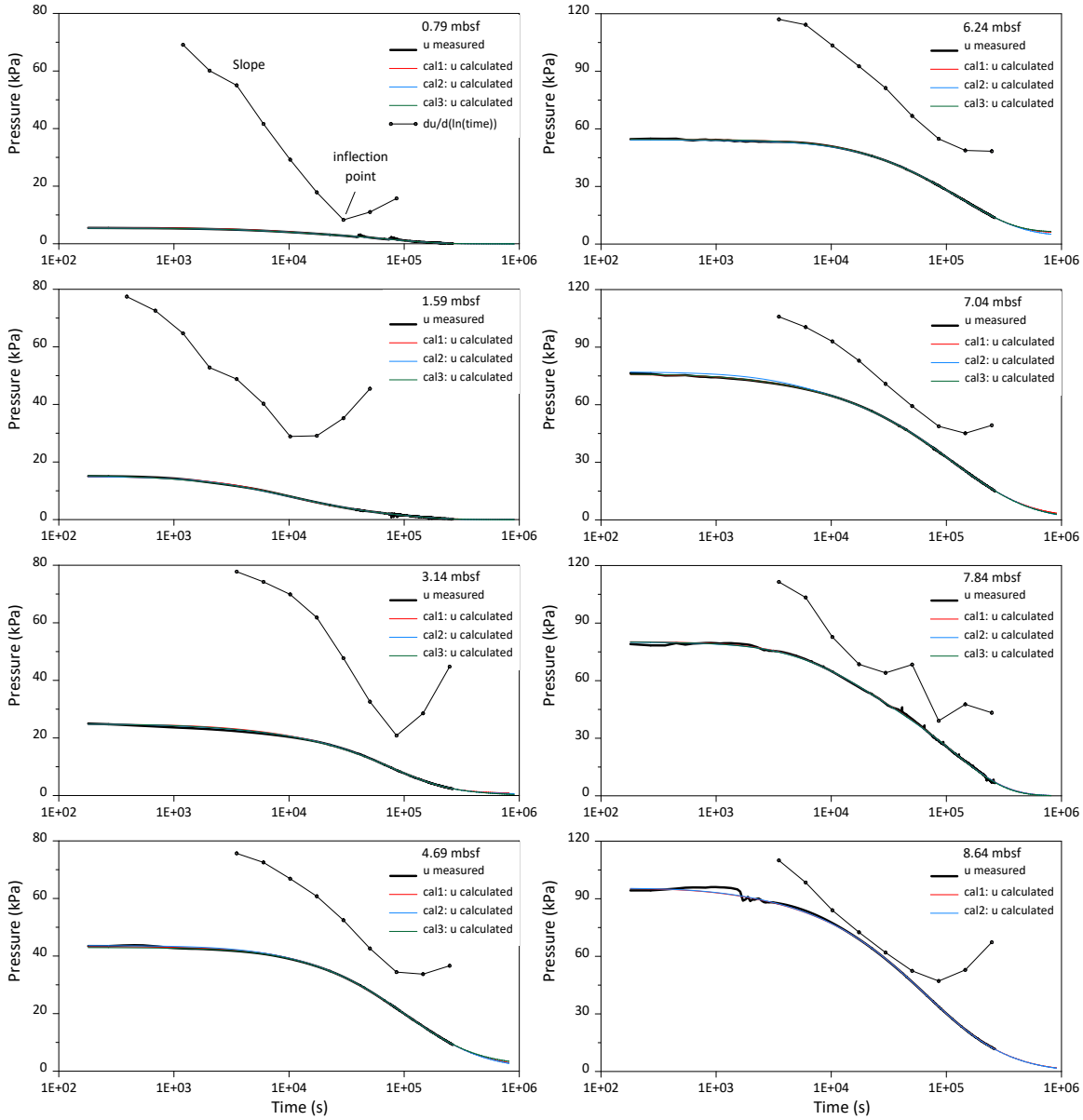

Figure S10. Pzm12W. Three runs for each sensor with three different set of parameters giving similar pore-water dissipation curves. The full range of pore-water pressure dissipation data are also plotted (black line). $\frac{\partial \Delta u}{\partial(\ln(t))}$ values are added to the diagram showing for some sensors the inflection point which corresponds to the $\left(\frac{\partial^2 \Delta u}{\partial ln(t)^2} > 0\right)$ criteria.

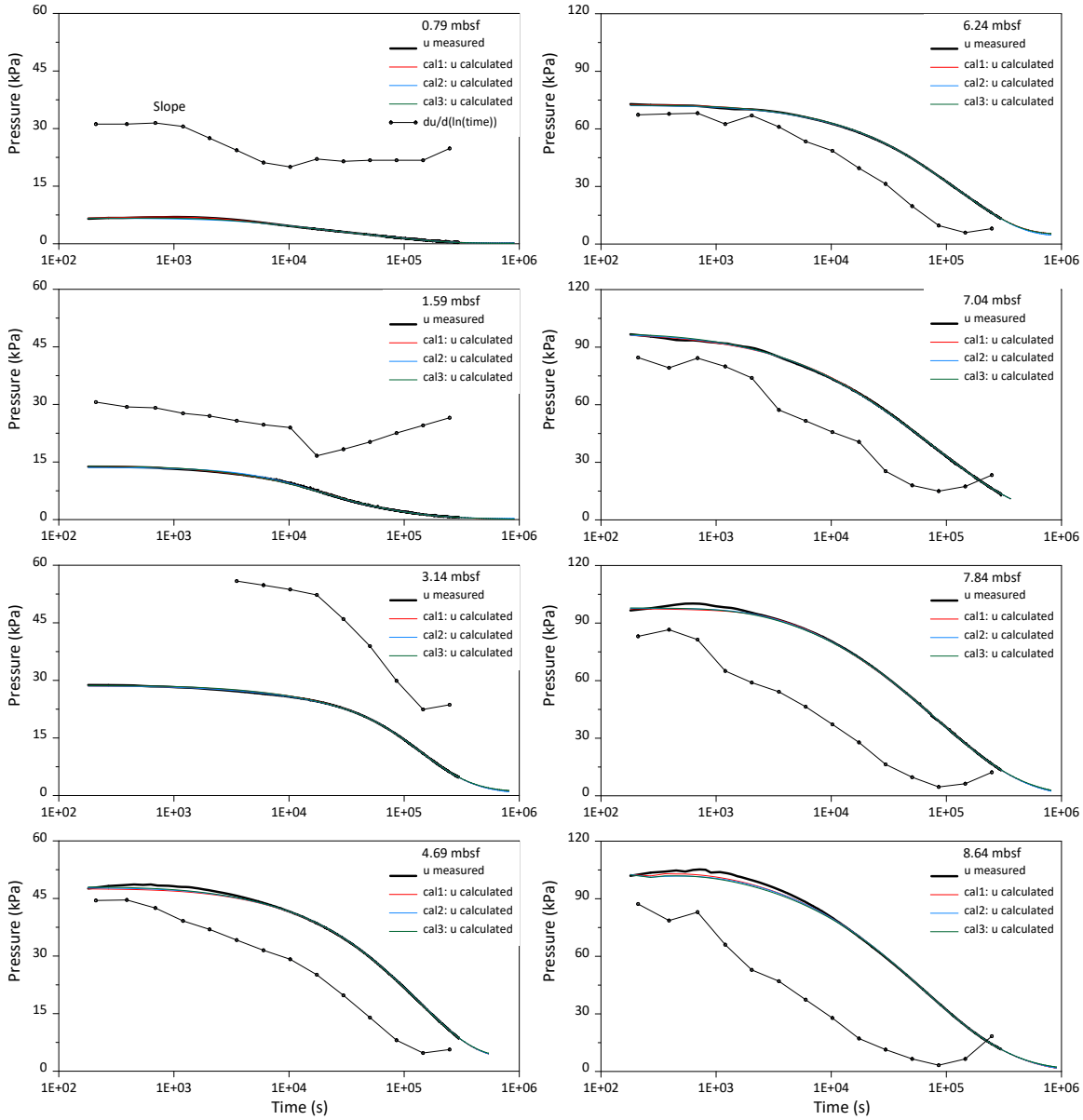

Figure S11. Pzm12E. Three runs for each sensor with three different set of parameters giving similar pore-water dissipation curves. The full range of pore-water pressure dissipation data are also plotted (black line). $\frac{\partial \Delta u}{\partial(\ln(t))}$ values are added to the diagram showing for some sensors the inflection point which corresponds to the $\left(\frac{\partial^2 \Delta u}{\partial ln(t)^2} > 0\right)$ criteria.

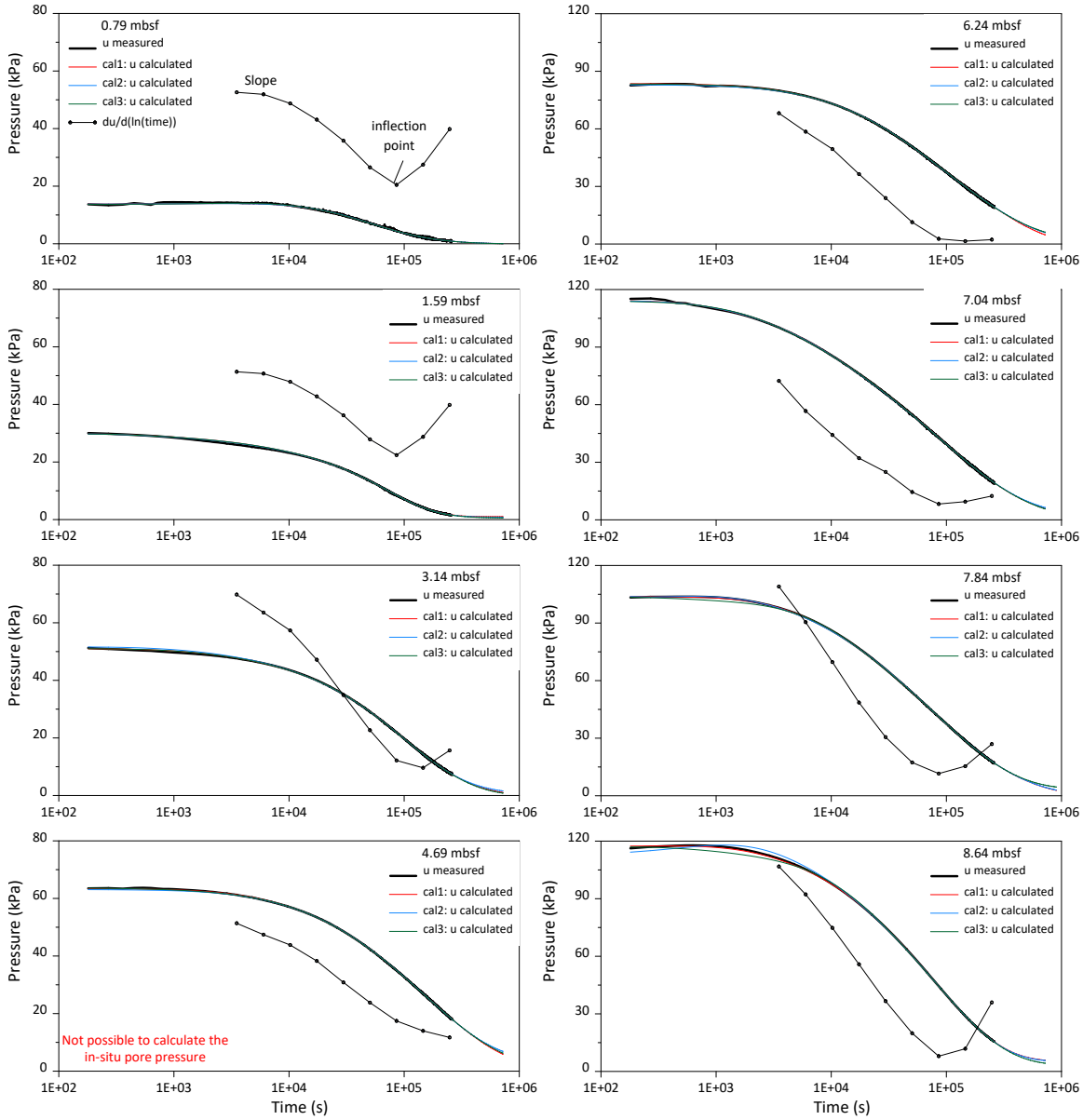

Figure S12. Pzm4W. Three runs for each sensor with three different set of parameters giving similar pore-water dissipation curves. The full range of pore-water pressure dissipation data are also plotted (black line). $\frac{\partial \Delta u}{\partial(\ln(t))}$ values are added to the diagram showing for some sensors the inflection point which corresponds to the $\left(\frac{\partial^2 \Delta u}{\partial ln(t)^2} > 0\right)$ criteria.

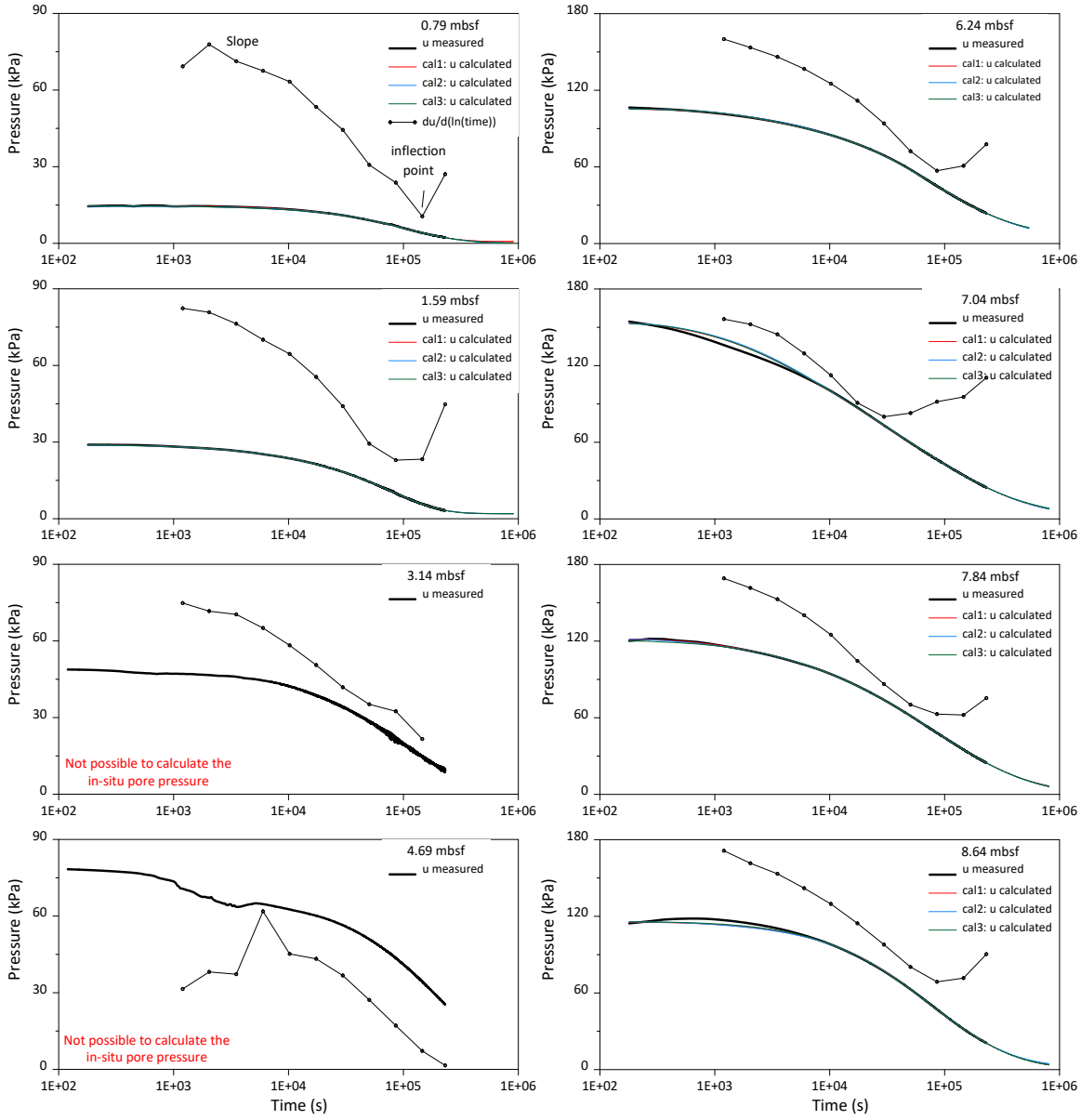

Figure S13. Pzm4E. Three runs for each sensor with three different set of parameters giving similar pore-water dissipation curves. The full range of pore-water pressure dissipation data are also plotted (black line). $\frac{\partial \Delta u}{\partial(\ln(t))}$ values are added to the diagram showing for some sensors the inflection point which corresponds to the $\left(\frac{\partial^2 \Delta u}{\partial ln(t)^2} > 0\right)$ criteria.

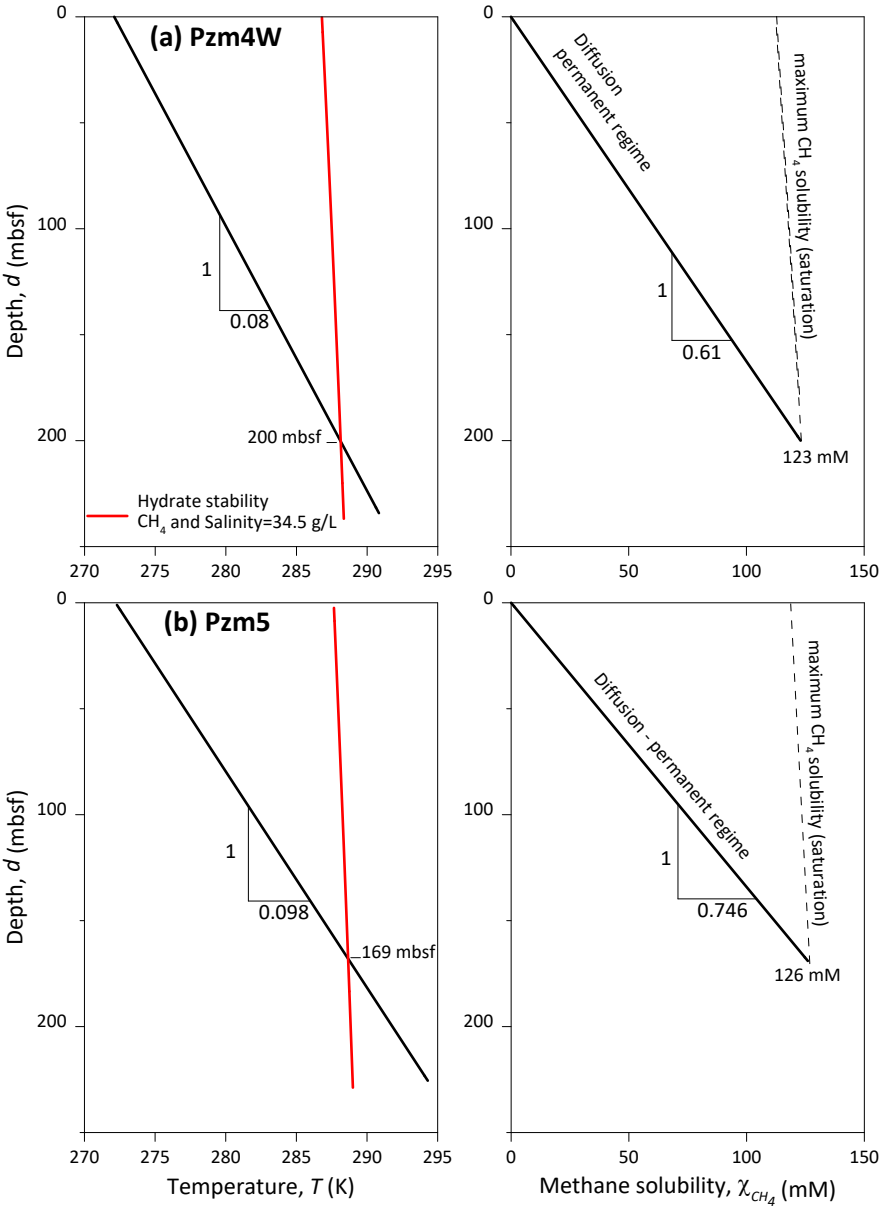

Figure S14. Methane solubility at sites (a) Pzm4E and (b) Pzm5.

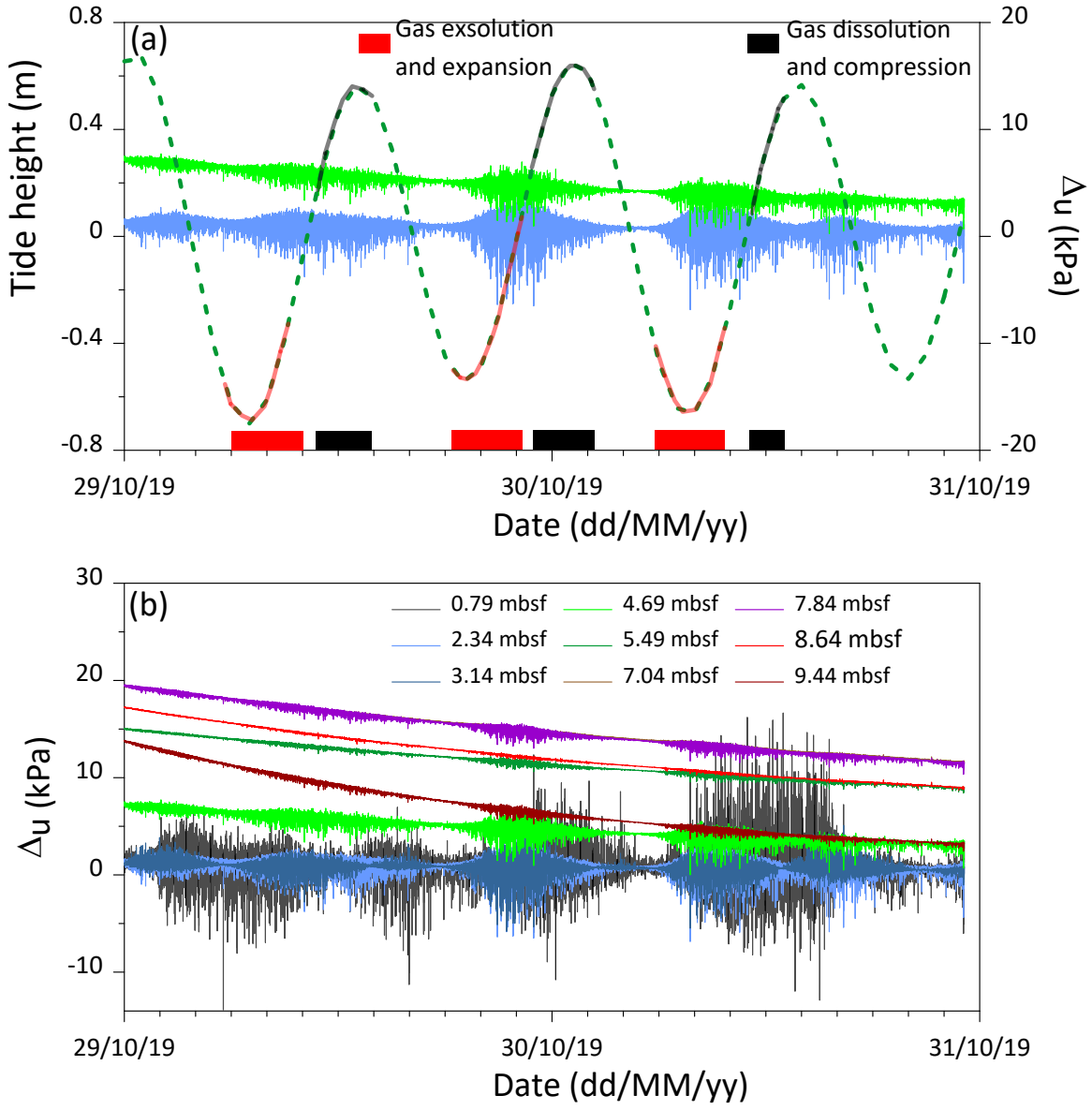

Figure S15. Site Pzm5 (a) Tidal height obtained at the piezometer location from the TPXO 9.0 global tidal model is shown as dashed line compared to Δu versus time at 3.14 and 4.69 mbsf. Red periods correspond to gas exsolution and expansion while black periods indicate gas dissolution and compression. (b) Δu versus time for the 9 sensors along Pzm5 showing Δu perturbations mainly during low and ascending tide cycles. The perturbation of Δu is proportional to the gas content [Garziglia et al., 2021].

Simplified name	Depth (m)	Station name	Quality
C-05	0.8	KH-05-PZM2	Very good
C-05	2.3	KH-05-PZM2	Very good
C-05	3.1	KH-05-PZM2	Good to Fair
C-05	5.49	KH-05-PZM2	Poor
C-05	8.6	KH-05-PZM2	Poor
C-05	9.4	KH-05-PZM2	Poor
C-12	0.84	KH-12-PZM3	-
C-12	2.3	KH-12-PZM3	Good to Fair
C-12	5.5	KH-12-PZM3	Poor

Table S1. Incremental loading oedometer tests carried out on sediment cores recovered from two investigated sites.

References

Abuel-Naga, H. M., and M. J. Pender (2012), Modified Terzaghi consolidation curves with effective stress-dependent coefficient of consolidation, *Géotechnique Letters*, *2*(2), 43-48.

Astm, D. (2004), 2435, *Standard Test Methods for One Dimensional Consolidation Properties of Soils using Incremental Loading*.

ASTM International (2006), Standard test method for one-dimensional consolidation properties of saturated cohesive soils using controlled-strain loading (Standard D4186–06), in Annual Book of ASTM Standards, vol. 04.08, Soil and Rock (I), pp. 1–15, West Conshohocken, Pa

Burns, S. E., and P. W. Mayne (1998), Monotonic and dilatory pore-pressure decay during piezocone tests in clay, *Canadian Geotechnical Journal*, *35*(6), 1063-1073.

Garziglia, S., N. Sultan, Y. Thomas, S. Ker, B. Marsset, X. Bompais, P. Woerther, C. Witt, A. Kopf, and R. Apprioual (2021), Assessing spatio-temporal variability of free gas in surficial cohesive sediments using tidal pressure fluctuations, *Journal of Geophysical Research: Earth Surface*, *126*(10), e2021JF006131.

Kim, Y., and S. R. Lee (2000), Prediction of long-term pore pressure dissipation behavior by short-term piezocone dissipation test, *Computers and Geotechnics*, *27*(4), 273-287.

Knies, J., and S. Vadakkepuliyambatta (2019), CAGE19-3 Cruise Report: Calypso giant piston coring in the Atlantic-Arctic gateway–Investigation of continental margin development and effect of tectonic stress on methane release, *CAGE–Centre for Arctic Gas Hydrate, Environment and Climate Report Series*, *7*.

Lunne, T., and M. Long (2006), Review of long seabed samplers and criteria for new sampler design, *Marine Geology*, *226*(1-2), 145-165.

Spivey, J. P., W. D. McCain, and R. North (2004), Estimating density, formation volume factor, compressibility, methane solubility, and viscosity for oilfield brines at temperatures from 0 to 275 C, pressures to 200 MPa, and salinities to 5.7 mole/kg, *Journal of Canadian Petroleum Technology*, *43*(07).

Sultan, N., and S. Lafuerza (2013), In situ equilibrium pore-water pressures derived from partial piezoprobe dissipation tests in marine sediments, *Canadian Geotechnical Journal*, *50*(12), 1294-1305.